Order by Disorder from Nonmagnetic Impurities in a Two-Dimensional Quantum Spin Liquid

Stefan Wessel,[1] B. Normand,[2] M. Sigrist,[3] and Stephan Haas[1]

[1]*Department of Physics and Astronomy, University of Southern California, Los Angeles, California 90089-0484*
[2]*Theoretische Physik III, Elektronische Korrelationen und Magnetismus, Universität Augsburg, D-86135 Augsburg, Germany*
[3]*Yukawa Institute for Theoretical Physics, Kyoto University, Kyoto 606-8502, Japan*

(Received 17 July 2000)

We consider doping of nonmagnetic impurities in the spin-1/2, 1/5-depleted square lattice. This structure, whose undoped phase diagram offers both magnetically ordered and spin-liquid ground states, is realized physically in CaV_4O_9. Doping into the ordered phase results in a progressive loss of order, which becomes complete at the percolation threshold. By contrast, doping into the spin liquids creates a phase of weak but long-ranged antiferromagnetic order, a true order-by-disorder phenomenon. We study the phase diagram of the doped system by computing the static susceptibility and staggered magnetization using a stochastic series-expansion quantum Monte Carlo technique.

DOI: 10.1103/PhysRevLett.86.1086 PACS numbers: 75.10.Jm, 75.30.Hx

Doping of low-dimensional quantum spin liquids leads to a variety of phenomena, including unconventional superconductivity when localized spins are replaced by mobile holes [1], and effective random spin systems, whose low-temperature properties are dominated by large effective spin degrees of freedom, in the presence of static impurities [2–4]. Such low-temperature phases have been observed recently in quasi-one-dimensional (quasi-1D) spin systems. In the two-leg ladder compound $Sr_xCa_{14-x}Cu_{24}O_{41+\delta}$, a superconducting transition has been measured at high pressure [5]. Zn doping of the quasi-1D ladder material $SrCu_2O_3$ [6], and of the dimerized chain $CuGeO_3$ [7], yields low-temperature phases with weak antiferromagnetic (AF) order, arising from effective couplings of random strength and sign between unpaired spins [4].

The question naturally arises of whether similar phenomena can be expected in quasi-2D systems. There are several prominent examples of 2D spin liquids including (i) structurally frustrated materials, such as $SrCu_2(BO_3)_2$ [8], containing AF coupled spin-1/2 triangles; (ii) interaction-frustrated systems, such as the J_1-J_2 Heisenberg model on a square lattice [9] in the gapped regime around $J_2/J_1 = 0.5$; and (iii) structurally discretized materials, such as the 1/5-depleted AF square lattice formed by the spin-1/2 vanadium ions of CaV_4O_9 (Fig. 1) [10]. These systems have resonant-valence-bond (RVB) ground states with a finite spin gap. Their AF correlation length is finite, decreasing with increasing gap size, and the low-temperature uniform susceptibility is exponentially activated. Nonmagnetic impurities in such systems induce a long-ranged AF order which is carried by effective spin degrees of freedom associated with each impurity, on the background of the dominant, gapped spin-liquid phase. This order arising from disorder, and the elimination of quantum phase transitions by the disorder, are the central results of our study. As in the quasi-1D case [11], the origin of AF ordering lies in the unfrustrated nature of the exponentially weak interactions between unpaired spins introduced when impurities break the RVB singlet units in a bipartite lattice: these are ferromagnetic when the free spins lie on the same sublattice and AF for opposite sublattices [3].

In this work we consider the effects of nonmagnetic impurities in the 1/5-depleted square lattice geometry (Fig. 1) motivated by the structure of CaV_4O_9 and by the possibility of doping this particular material with Ti. While frustrated couplings are important in CaV_4O_9 [12,13], an effective model of simply coupled plaquettes remains valid for impurity effects. First, we present a theoretical analysis for the unfrustrated system, which contains all the qualitative features we wish to address, and return thereafter to the experimental situation.

The effective magnetic Hamiltonian,

$$H = J \sum_{\square} \mathbf{S}_i \cdot \mathbf{S}_j + J' \sum_{\square - \square} \mathbf{S}_i \cdot \mathbf{S}_j , \qquad (1)$$

is a spin-1/2 AF Heisenberg model where J is the intraplaquette and J' the interplaquette exchange coupling constant, in which the sums marked by $\square$ and $\square - \square$

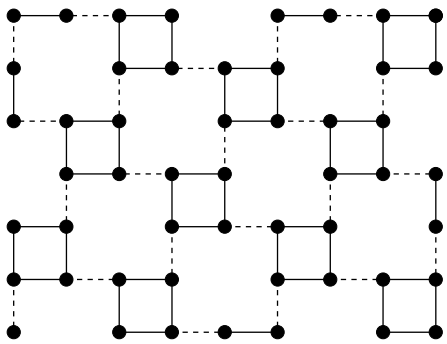

FIG. 1. The 1/5-depleted square lattice. Intraplaquette couplings J are indicated by solid lines, and interplaquette couplings J' by dashed lines.

 0031-9007/01/86(6)/1086(4)$15.00

run over nearest neighbors within and between the plaquettes. The undoped phase diagram contains a spin-liquid plaquette RVB (PRVB) phase for $J'/J \lesssim 0.93$, an AF-ordered phase in the interval $J'/J \in [0.93, 1.68]$, and a further spin liquid, the dimer RVB (DRVB) phase, at $J'/J \gtrsim 1.68$ [14]. Impurity effects on the quantum transitions between these phases are an important feature of our study. Expansions about the plaquette and dimer limits will be compared with simulations using the stochastic series-expansion quantum Monte Carlo (SSE QMC) algorithm [15], on 1/5-depleted, square lattices of up to 30×30 sites, and at temperatures down to $T = 0.02J$. This algorithm involves expansion of the partition function in inverse temperature, employs local and global system updates, and is significantly more efficient than conventional QMC schemes. In the presence of nonmagnetic impurities, ensemble averages over 500 random realizations were taken to ensure numerical errors smaller than the symbol sizes in Figs. 2 and 3.

Considering first an ensemble of completely decoupled four-spin plaquettes, a small number of randomly placed, nonmagnetic dopants creates free spin-1/2 moments, corresponding to the doubly degenerate $S^z = \pm 1/2$ ground state of three-spin Heisenberg clusters [16]. Each of these "pruned" plaquettes introduces a low-lying state within the spin gap and gives a paramagnetic contribution to the susceptibility $\chi(T)$ at low temperature. Upon further doping, clusters containing $n < 3$ spins are also created, with distributions $P(n)$ [17], but only unpaired spins contribute to the low-T Curie tail. Figure 2(a) shows $T\chi(T)$ for various impurity concentrations. Without impurities, this quantity extrapolates exponentially to zero as the temperature is lowered, indicative of the spin gap in the clean system. With impurities, the zero-temperature Curie constant

$$C = \lim_{T\to 0}[T\chi(T)] = \frac{1}{4}\left(\frac{P(1) + P(2)/3 + P(3)}{1 - \rho}\right) \quad (2)$$

depends on concentration as shown in the inset of Fig. 2(a). For all ρ, three distinct temperature regimes are observed. (i) For $T \gg \Delta_{\max}$ (not shown) the spins are essentially independent, each contributing $\frac{\mu_B^2}{4k_B}$ to C. $\Delta_{\max} = 1.5J$ is the largest energy level separation in any cluster. (ii) For $\Delta_{\min} < T < \Delta_{\max}$, some spins freeze into singlets, gradually reducing the overall magnetic response by a factor of approximately ρ as T decreases. $\Delta_{\min} = 0.25J$ is the smallest energy spacing in any cluster. (iii) For $T < \Delta_{\min}$, plateaus appear in $T\chi(T)$ when the contributing clusters reach their ground states.

With finite interplaquette coupling, spin-1/2 moments on adjacent plaquettes may combine to form new RVB clusters with smaller spin gaps, involving larger numbers of spins. In the susceptibility, this effective recombination reduces C from its value for decoupled, pruned plaquettes, further suppressing $T\chi(T)$ at very low T. This cluster formation may be quantified from the distribution functions for neighboring plaquettes, evaluated perturbatively in J'/J. These functions have a nontrivial dependence on the relative positions of the dopant vacancies in adjacent clusters. Close to the PRVB limit, the inset of Fig. 2(a) illustrates this reduction of C, which is strongest at smaller ρ where more spins are available to form larger RVB clusters. Figure 2(b) shows analogous results for the DRVB limit.

In Fig. 3, the T-dependence of the uniform susceptibility is shown at various doping levels in the three regimes

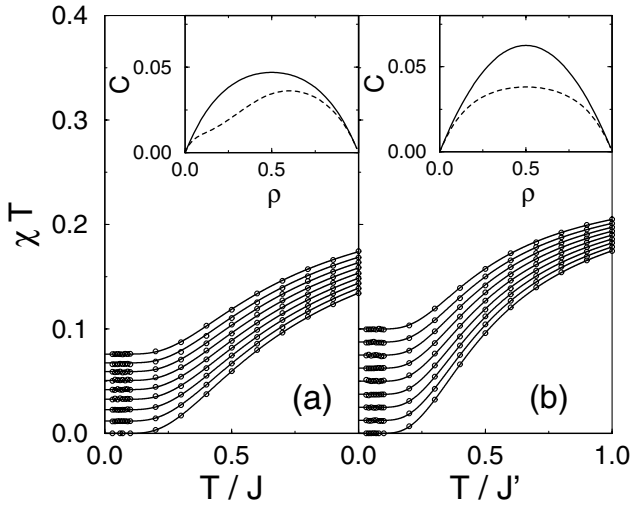

FIG. 2. (a) Ensemble of decoupled plaquettes: temperature dependence of $T\chi(T)$ at impurity concentrations $\rho = 0.0, 0.05, \ldots, 0.4$. Solid lines are exact results, and symbols are QMC simulations. $T\chi(T)$ is normalized by the number of spins in the system. (b) As (a), for decoupled dimers. Insets: Dependence of zero-temperature Curie constant C on ρ. Solid lines denote decoupled plaquette and dimer limits, and dashed lines the results from perturbation expansion with (a) $J'/J = 0.1$ and (b) $J/J' = 0.1$.

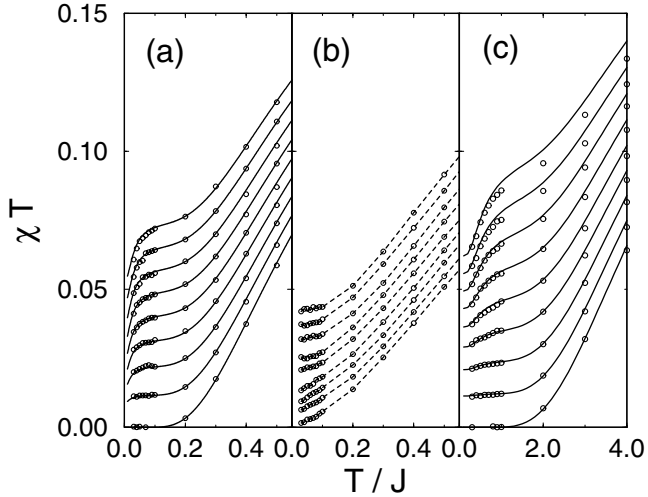

FIG. 3. Temperature dependence of $T\chi(T)$ at impurity concentrations $\rho = 0.0, 0.05, \ldots, 0.4$. (a) PRVB regime, $J'/J = 0.3$; (b) ordered AF regime, $J'/J = 1.2$; (c) DRVB regime, $J'/J = 2.0$. Solid lines are results from expansions about the decoupled limits, and symbols are from SSE QMC simulations. Dashed lines in (b) are guides to the eye.

of J'/J. In Figs. 3(a) and 3(c), results from SSE QMC simulations (symbols) are plotted along with those from perturbative expansions about the limits of decoupled plaquettes and dimers (solid lines). At $\rho = 0$, $T\chi(T)$ clearly displays activated behavior in the two gapped regions but a linear form in the long-range-ordered phase.

PRVB.—At small ρ, a plateau develops in $T\chi(T)$ at low temperatures, $T \sim \Delta_{\min}$, indicating a freezing of the plaquettes into their ground state configurations. For a finite interplaquette coupling, the additional reduction of C observed at ultralow temperatures indicates that the plaquette spins become correlated on an ultralow energy scale J_{eff}. At sufficiently small ρ, this energy can be estimated [3] by assuming RKKY-like interactions between impurity spins with separation $\mathbf{r}_i = (i_x, i_y)$, yielding

$$J_{\text{eff}}(\mathbf{0}, \mathbf{r}_i) \approx J(-1)^{(i_x+i_y-1)} \exp\left(-\frac{(1-\rho)}{\xi_{\text{AF}}(\rho, T)}\right), \quad (3)$$

where ξ_{AF} is the short-range AF correlation length in the spin-liquid regimes. Approaching $T = 0$, the Curie constant extrapolates to $C = \rho/12$, a reduction of roughly $1/3$ compared to the plateau value [3]. At larger impurity concentrations, the onset of this ultralow-T regime moves up, consistent with $T \sim J_{\text{eff}}$ [Eq. (3)]. At still higher doping, the picture of isolated impurity spins and RKKY interactions mediated via the spin-liquid RVB background breaks down. The regimes of moment formation and correlation overlap, and the plateau feature in $T\chi(T)$ becomes less pronounced. On doping towards the percolation threshold ρ_c, the magnetic response is dominated by the largest percolation clusters, typically containing several pruned plaquettes. From simulations in the classical limit [18], we find $\rho_c = 0.26(9)$ for the $1/5$-depleted lattice. Studies of percolation thresholds in regular square lattices suggest that the value of ρ_c for the quantum spin system differs by less than 1% from the classical value ($\rho_c = 0.407$ [18]). In this regime the plaquette plateaus disappear, a trend accentuated as the long-range-ordered regime is approached ($J'/J \to 0.93$), where ξ_{AF} increases and [Eq. (3)] the onset of the ultralow-T regime moves to lower energies.

DRVB.—As in the PRVB regime, nonmagnetic impurities introduce local moments in the gapped, spin-liquid state. A dimer "plateau" is reached at $T \sim J_{\text{eff}}$, and further moment recombination occurs at ultralow temperatures, leading to an additional reduction of $T\chi(T)$ as $T \to 0$. The plateaus disappear on approaching the transition to the AF phase, $J'/J \to 1.68^{+}$.

AF.—In contrast to gapped spin liquids, isolated, nonmagnetic impurities do not introduce quasifree local moments, because all spins remain aligned with the staggered AF background [19]. However, the low-temperature susceptibility does have a divergent contribution, albeit with C smaller than in the spin liquids at given ρ, due to free moments isolated from the AF system by dopants.

Returning to the issue of order by disorder, our simulations close to the AF regime of the pure system show that introduced moments do not simply recombine into larger RVB clusters but form a long-range-ordered AF network at ultralow temperatures. This doping-induced long-range order is best characterized by the staggered magnetization m_s, which is shown in Fig. 4 as a function of nonmagnetic impurity doping within each of the distinct phases of the system. As also in Fig. 5, these data were obtained by finite-size extrapolation at ultralow temperatures and thus represent the thermodynamic limit [14]. In the long-range-ordered AF regime, we see that random static vacancies simply reduce the average staggered magnetization, driving it to zero beyond the percolation threshold $\rho_c = 0.26(9)$. By contrast, in the spin-liquid regimes the doping-induced moments have random effective interactions mediated by the RVB background. These interactions are *unfrustrated*, since they arise from the mere depletion of an unfrustrated, bipartite AF Heisenberg model [3]. A long-ranged order may then be expected to emerge from the large-spin clusters at zero temperature. Indeed, the resulting AF network has an extensive staggered magnetization, which peaks around $\rho = 0.08$. This ordered AF phase coexists [11] with the gapped, spin-liquid state of the majority, undoped plaquettes or dimers (Fig. 3). The mechanism leading to this moment formation may be viewed as an order-by-disorder phenomenon. The inset of Fig. 4 shows the staggered magnetization as a function of the coupling ratio at the maximal doping. The disorder-induced, ordered moments in the spin-liquid regions are significant over a wide range of J'/J and become large near the phase boundaries of the pure system, where they cross continuously to the full moment of the intrinsically ordered regime.

Our results are summarized by the phase diagram in Fig. 5, where the shading illustrates the strength of the

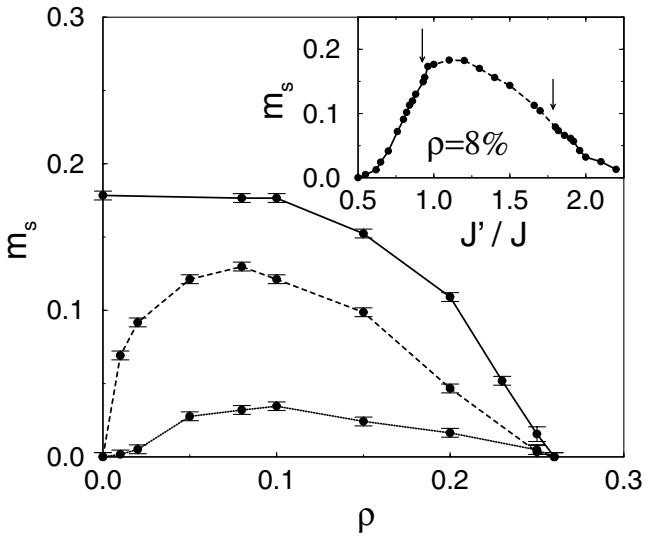

FIG. 4. Staggered magnetization as a function of impurity doping for coupling ratios J'/J in the PRVB (dashed line), ordered (solid line), and DRVB (dotted line) regimes, normalized to 0.5 for Néel order. The inset shows the evolution of m_s with J'/J at a fixed doping $\rho = 8\%$; arrows indicate the phase boundaries of the pure system.

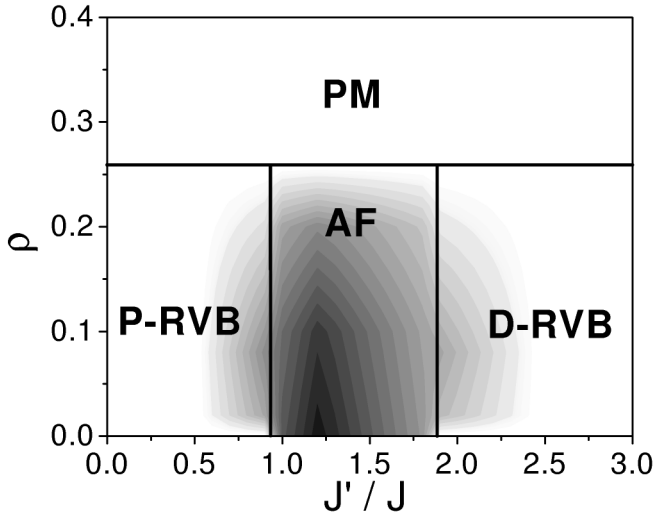

FIG. 5. Phase diagram for the 1/5-depleted, square-lattice antiferromagnet with doping by nonmagnetic impurities.

staggered magnetic order. The solid lines depict quantum phase boundaries only of the pure systems. At any finite doping below the percolation threshold, there is a "smearing" of the transitions as the impurity-induced AF order within the spin liquid crosses smoothly to impurity-suppressed order within an AF. Impurities may be considered as damaging both to the AF ordered phase, simply by diminishing m_s, and to the quantum spin-liquid phase, in the sense of introducing states within the gap, which at sufficiently low temperatures become correlated.

Experimentally, the situation in CaV_4O_9 is more complex than that simulated here. Inelastic neutron scattering measurements [12], and subsequent simulations [13], show that the magnetic system is composed of metaplaquettes (squares of side $\sqrt{2}$ larger than the smallest V-V separation) with $J_2 = J = 14$ meV, which interact with their neighbors via mutually frustrating couplings $J_1 = J_1' = 0.49J$ and with next neighbors by a further weak coupling $J_2' = 0.25J$. The frustrated nature of J_1 implies that the effective coupling J' between metaplaquettes is small, and thus that the physical system can be described by the model (1) of Fig. 1 in the PRVB regime; this deduction is consistent with the robust spin gap, $\Delta = 9.4$ meV, of CaV_4O_9. Doping by nonmagnetic impurities could be effected by random replacement of some spin-1/2 V^{4+} ions with Ti^{4+}. Our simulations of the uniform susceptibility and staggered magnetization suggest that induced AF order should be detectable in 5%–10% Ti-doped CaV_4O_9, by measurements of $\chi(T)$, Knight shift or magnetic Bragg scattering.

In summary, we have analyzed the behavior on doping by nonmagnetic impurities of the spin liquid and ordered AF phases of the Heisenberg model on a 1/5-depleted, square lattice of spins $S = 1/2$. In the spin liquids, introduction of impurities creates effectively free spins which combine through random, unfrustrated interactions to create a long-ranged AF order at $T = 0$ in the background of the gapped, spin-liquid phase. In the intrinsically AF regime, impurities cause a progressive destruction of the long-range order until it vanishes at the percolation threshold. The sharp quantum phase transitions between the two spin-liquid phases and the AF-ordered phase in this model cease to exist in the impurity-doped case, and AF order extends exponentially into the spin-liquid regime. The unique magnetic plaquette structure of CaV_4O_9 provides a well-defined starting point for studying the effect of nonmagnetic impurities in spin liquids and yields valuable insight for other 2D RVB compounds. Nevertheless, it must be noted that for systems with frustrating interactions, the effective interactions tend also to be frustrated, and the resulting order may then exhibit glassy features.

We acknowledge financial support from NSF Grant No. DMR 0089882 (S. W., S. H.), SFB 484 of the Deutsche Forschungsgemeinschaft (B. N.), and the Japanese Ministry of Education and Science (M. S.).

[1] E. Dagotto, J. Riera, and D. J. Scalapino, Phys. Rev. B **45**, 5744 (1992); E. Dagotto and T. M. Rice, Science **271**, 618 (1996).
[2] E. Westerberg *et al.,* Phys. Rev. Lett. **75**, 4302 (1995).
[3] M. Sigrist and A. Furusaki, J. Phys. Soc. Jpn. **65**, 2385 (1996).
[4] S. Haas, J. Riera, and E. Dagotto, Phys. Rev. B **48**, 13 174 (1993).
[5] M. Uehara *et al.,* J. Phys. Soc. Jpn. **65**, 2764 (1996).
[6] M. Azuma *et al.,* Phys. Rev. B **55**, R8658 (1997).
[7] Y. Sasago *et al.,* Phys. Rev. B **54**, R6835 (1996).
[8] H. Kageyama *et al.,* Phys. Rev. Lett. **82**, 3168 (1999).
[9] E. Dagotto and A. Moreo, Phys. Rev. B **39**, 4744 (1989).
[10] S. Taniguchi, T. Nishikawa, Y. Yasui, Y. Kobayashi, M. Sato, T. Nishioka, M. Kontani, and K. Sano, J. Phys. Soc. Jpn. **64**, 2758 (1995).
[11] H. Fukuyama, T. Tanimoto and M. Saito, J. Phys. Soc. Jpn. **65**, 1182 (1996).
[12] K. Kodama *et al.,* J. Phys. Soc. Jpn. **66**, 793 (1997).
[13] Y. Fukumoto and A. Oguchi, J. Phys. Soc. Jpn. **67**, 697 (1998); Z. Weihong, J. Oitmaa, and C. J. Hamer, Phys. Rev. B **58**, 14 147 (1998); M. Mambrini and F. Mila, Physica (Amsterdam) **259B–261B**, 967 (1999).
[14] M. Troyer, H. Kontani, and K. Ueda, Phys. Rev. Lett. **76**, 3822 (1996).
[15] A. W. Sandvik and J. Kurkijärvi, Phys. Rev. B **43**, 5950 (1991); A. Sandvik, Phys. Rev. B **59**, R14 157 (1999).
[16] M. Laukamp *et al.,* Phys. Rev. B **57**, 10 755 (1998).
[17] $P(n) = 4!\,\rho^{(4-n)}(1-\rho)^n/[n!\,(4-n)!]$ by standard combinatorial analysis.
[18] D. Stauffer and A. Aharony, *Introduction to Percolation Theory* (Taylor & Francis, London, 1992).
[19] A. W. Sandvik, E. Dagotto, and D. J. Scalapino, Phys. Rev. B **56**, 11 701 (1997).